Research Article | Vol. 32, No. 17 / 12 Aug 2024 / Optics Express 29138
Optics EXPRESS

Advancing LWIR FSO communication through high-speed multilevel signals and directly modulated quantum cascade lasers

MAHDIEH JOHARIFAR,[1,8] LAURELINE DURUPT,[2] HAMZA DELY,[3] ARMANDS OSTROVSKIS,[4] RICHARD SCHATZ,[1] RAFAEL PUERTA,[1,5] GREGORY MAISONS,[2] TOMS SALGALS,[4] DJAMAL GACEMI,[3] LU ZHANG,[6] SANDIS SPOLITIS,[4] YAN-TING SUN,[1] VJAČESLAVS BOBROVS,[4] XIANBIN YU,[6] ANGELA VASANELLI,[3] OSKARS OZOLINS,[1,4,7] CARLO SIRTORI,[3] AND XIAODAN PANG[1,4,7,9]

[1]*Department of Applied Physics, KTH Royal Institute of Technology, 106 91 Stockholm, Sweden*
[2]*mirSense, 2 Bd Thomas Gobert, 91120 Palaiseau, France*
[3]*Laboratoire de Physique de l'ENS, Département de Physique, École Normale Supérieure, Université PSL, Sorbonne Université, Université Paris Cité, CNRS, 75005 Paris, France*
[4]*Institute of Telecommunications, Riga Technical University, 1048 Riga, Latvia*
[5]*Ericsson Research, Ericsson AB, 164 83 Stockholm, Sweden*
[6]*College of Information Science and Electrical Engineering, Zhejiang University, Hangzhou 310027, China*
[7]*RISE Research Institutes of Sweden, 164 40 Kista, Sweden*
[8]*mahdieh@kth.se*
[9]*xiaodan@kth.se*

Abstract: This study investigates the potential of long-wave infrared (LWIR) free-space optical (FSO) transmission using multilevel signals to achieve high spectral efficiency. The FSO transmission system includes a directly modulated-quantum cascade laser (DM-QCL) operating at 9.1 µm and a mercury cadmium telluride (MCT) detector. The laser operated at the temperature settings of 15°C and 20°C. The experiment was conducted over a distance of 1 m and in a lab as a controlled environment. We conduct small-signal characterization of the system, including the DM-QCL chip and MCT detector, evaluating the end-to-end response of both components and all associated electrical elements. For large-signal characterization, we employ a range of modulation formats, including non-return-to-zero on-off keying (NRZ-OOK), 4-level pulse amplitude modulation (PAM4), and 6-level PAM (PAM6), with the objective of optimizing both the bit rate and spectral efficiency of the FSO transmission by applying pre- and post-processing equalization. At 15°C, the studied LWIR FSO system achieves net bitrates of 15 Gbps with an NRZ-OOK signal and 16.9 Gbps with PAM4, both below the 6.25% overhead hard decision-forward error correction (6.25%-OH HD-FEC) limit, and 10 Gbps NRZ-OOK below the 2.7% overhead Reed-Solomon RS(528,514) pre-FEC (KR-FEC limit). At 20°C, we obtained net bitrates of 14.1 Gbps with NRZ-OOK, 16.9 Gbps with PAM4, and 16.4 Gbps with PAM6. Furthermore, we evaluate the BER performance as a function of the decision feedback equalization (DFE) tap number to explore the role of equalization in enhancing signal fidelity and reducing errors in FSO transmission. Our findings accentuate the competitive potential of DM-QCL and MCT detector-based FSO transceivers with digital equalization for the next generation of FSO communication systems.

#530228 https://doi.org/10.1364/OE.530228
Journal © 2024 Received 16 May 2024; revised 17 Jul 2024; accepted 17 Jul 2024; published 29 Jul 2024

Optics EXPRESS

1. Introduction

In response to the exponential growth of data traffic, sixth-generation (6 G) wireless communication technology is ready to supersede its predecessor, 5 G, and explore the frequencies extending into the millimeter-wave (mmWave) spectrum and beyond, with a focus on optimizing spectral efficiency and data throughput [1,2]. The inherent atmospheric transmission characteristics of mid-infrared (MIR) radiation emerge as a promising avenue for enhancing the resilience and performance of 6 G systems, particularly in facilitating long distance free-space optical (FSO) communications with heightened reliability and throughput capabilities [3,4]. FSO transmissions face several technical challenges, including beam divergence over long distances, pointing errors requiring precise alignment, significant atmospheric attenuation in unclear weather, and atmospheric turbulence. While solutions exist for divergence, alignment, and attenuation, atmospheric turbulence remains largely unsolved [5]. Atmospheric turbulence degrades FSO link performance in a distance of over 1 km. Fluctuations in the atmosphere's temperature and pressure cause variations in the refractive index along the transmission path, leading to fluctuations in signal quality. These fluctuations increase error probabilities, thereby limiting system performance [6].

MIR wavelengths (2.5 - 25 μm) are at the crossroads of optics and electronics, emerging as pivotal components for many applications spanning from spectroscopy and chemical sensing to thermal imaging and communications [7,8]. The medium-wave infrared (MWIR, 3-5 μm, 60–100 THz) and the long-wave infrared (LWIR, 8-12 μm, 25–37 THz) segments are the two atmospheric transmission windows situated within the MIR region that are considered promising candidates for future FSO communications [9,10]. The MWIR and LWIR encounter notably reduced Mie scattering, compared with the near-IR telecom band around 1.5 μm, particularly factoring in particles commonly present in various meteorological phenomena such as dust, sand, haze, and low-altitude clouds [11,12]. Due to their longer wavelengths, MWIR and LWIR exhibit elevated resistance against atmospheric turbulence scintillation. Semiconductor optoelectronic components that emit MIR directly offer an alternative for reduced footprint, cost-effectiveness, and improved integrability [13,14]. Recent advancements in quantum optoelectronic devices, like quantum cascade lasers (QCLs), with features such as continuous-wave operation at room temperature, high output power, and broad modulation bandwidth, show capacity for MIR FSO transceiver development [15]. However, the inherent hardware complexity and high power consumption can impede practical development. QCLs require high power consumption, with most input power dissipated as heat. This necessitates robust cooling systems to manage their operating temperature [16]. Despite these challenges, there have been dedicated efforts to enhance the energy consumption of QCLs [17]. Several MWIR and LWIR FSO systems with multi-gigabit transmission rates have been reported with QCL and different types of detectors, including quantum cascade detector (QCD), quantum-well IR detectors (QWIP), and HgCdTe (mercury cadmium telluride, MCT) detector [18–23]. Particularly, MCT detectors operate across a wider spectral range, covering both MWIR and LWIR, which can potentially facilitate wavelength division multiplexing (WDM) without the necessity for a dedicated detector design per wavelength, and simplify the implementation of multi-channel communication systems, and enhance flexibility in network configurations [24]. MCT detectors with wide spectral coverage show decreased peak detectivity due to increased noise and lower quantum efficiency and typically range from 10^8 to 10^9 cm·Hz$^{1/2}$.W^{-1}. In contrast, MCTs with narrower spectral ranges achieve higher detectivity, often exceeding 10^9 cm·Hz$^{1/2}$.W^{-1}. In addition, broad spectral coverage introduces more noise, particularly in LWIR, lowering overall detectivity, whereas narrower spectral ranges enhance detectivity by reducing noise [25]. Despite of relatively narrower bandwidth, MCT detectors' high responsivity and low noise level can elevate the signal-to-noise ratio (SNR), suggesting the feasibility of multilevel signal transmissions, such as 4-level pulse amplitude modulation (PAM4) and PAM6, to boost the FSO system's spectral efficiency. Han et al. [21] reported a bandwidth of approximately 750 MHz for MCT, the detector from our

Optics EXPRESS

previous work, with a responsivity of 2.5 $A.W^{-1}$. Hakl et al. [20] achieved a bandwidth of around 26.5 GHz in practical settings for the QWIP, and the responsivity of 100 $mA.W^{-1}$. The bandwidth for QCDs for Dely et al. [19] and Joharifar et al. [23] is about 6 GHz, primarily limited by factors such as electrical parasitic capacitance from the mesa structure, packaging, and driving circuits, and has a responsivity of 4.5 $mA.W^{-1}$. By integrating digital equalization techniques such as decision feedback equalizer (DFE), the overall performance of the FSO system can be further enhanced. This strategic combination enhances the reliability and efficiency of data transmission, enabling FSO systems to maintain robust performance even in challenging channel conditions such as adverse weather, atmospheric turbulence, and variable light intensities [26]. Previously, we demonstrated the FSO transmission of an 8.1 Gbps signal using PAM8 through an LWIR QCL coupled with a low-bandwidth MCT detector [27]. Additionally, we successfully delivered 5 G New Radio (NR) signals via LWIR FSO transmission at 9.15 μm, in full compliance with the 3GPP RF conducted transmitter requirements [28].

In this work, we successfully transmit net bitrates of 16.9 Gbps PAM4 and 15 Gbps non-return-to-zero on-off keying (NRZ-OOK) signals with a bit error rate (BER) below the 6.25% overhead hard decision-forward error correction (6.25%-OH HD-FEC) limit, and 10 Gbps NRZ-OOK below the 2.7% overhead Reed–Solomon RS(528,514) pre-FEC (KR-FEC limit) at 15°C, and 14.1 Gbps NRZ-OOK, 16.9 Gbps PAM4, and 16.4 Gbps PAM6 signals at 20°C, utilizing an enhanced MCT photovoltaic detector with improved bandwidth to reinforce the end-to-end frequency response of the system over 1 m of distance in a lab [29]. The experiments were conducted at two different laser temperatures of 15°C and 20°C. At lower temperatures, the threshold current of a QCL is reduced because the carrier density needed for population inversion is achieved at a lower current. Internal losses, such as free carrier absorption and scattering, decrease, leading to a higher quality factor (Q-factor), higher output power, and a higher data rate. Quantum efficiency also improves at lower temperatures due to fewer phonon scatterings. As temperature increases, the emission wavelength of the QCL can shift, and the threshold current also increases, requiring more energy consumption [30]. The end-to-end 3-dB bandwidth increased from 170 MHz to 690 MHz compared to our previous work [21]. As a result, we achieved a net bitrate of 16.9 Gbps PAM4, which represents the highest demonstrated LWIR FSO transmission data rate using MCT detectors, surpassing our previous record of 8.1 Gbps PAM8, which was carried out in 1.4 m. It is worth noting distance was chosen for ease of implementation rather than as an upper limit. Furthermore, detailed digital pre- and post-equalization methods were employed to optimize signal quality, minimize distortion, and improve error rates.

2. Configuration and characterization of the system

2.1. Experimental setup of the FSO system

Figure 1 illustrates the experimental setup of the LWIR FSO transmission system. The data traces are digitally pre-processed at the transmitter and digitally post-processed at the receiver to obtain optimal system performance. Three modulation formats are employed in this experiment: NRZ-OOK, 4-level PAM (PAM4), and 6-level PAM (PAM6), which are generated offline using a digital signal processing (DSP) routine at the transmitter-side (Tx) on the lab computer. In the first stage of the Tx DSP routine, over a million samples of a repeated pseudorandom binary sequence (PRBS) are generated by MATLAB using the Mersenne Twister algorithm with a shuffled seed number. The PRBS samples are mapped onto the PAM symbols by incorporating PAM mapping, and then pulse shaped with a root-raised cosine (RRC) filter of 0.1 roll-off factor. Next, we conducted re-sampling to adjust the sampling rate of the signal to match that of the arbitrary waveform generator (AWG, 65 GSa/s) and prevent digital artifacts. A static 2-tap pre-emphasis finite impulse response (FIR) filter is used as the last stage, compensating for limitations in system bandwidth and improving the SNR by boosting the higher frequency components of the signal. After the Tx DSP, the digital samples are converted to the analog

Optics EXPRESS

domain by the AWG. The output signal from the AWG is electrically amplified within the range of 2 V_{pp} to 3.1 V_{pp}. Before passing on to the QCL mount, a high-current bias-tee with a 40 GHz RF bandwidth is used to combine the modulation signal with a DC current.

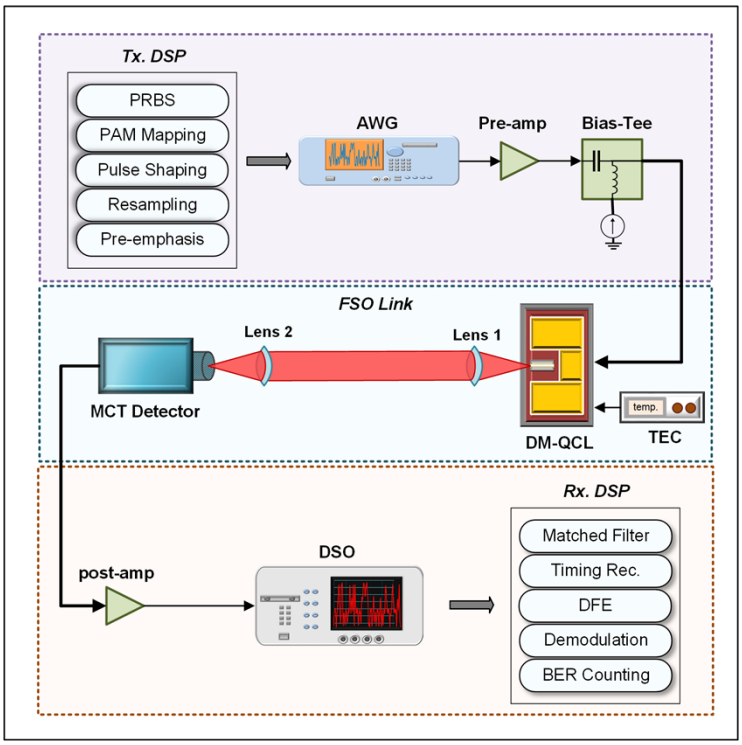

Fig. 1. Experimental setup with DSP routines in the transmitter and the receiver ends. PRBS: pseudorandom binary sequence; AWG: arbitrary waveform generator; TEC: temperature controller; DM-QCL: directly modulated-quantum cascade laser; MCT: mercury cadmium telluride; DSO: digital storage oscilloscope; DFE: decision-feedback equalizer; BER: bit error rate.

Two beam collimating lenses are installed: one positioned near the QCL mount to help with the optical beam alignment and to reduce divergence so that the beam can travel efficiently through the 1 m distance of the FSO link. The other is close to the photodetector (PD) to assist with the incoming light collection. On the receiving end, we used an IR power meter to calibrate and optimize the received signal power and then replaced it with a commercial MCT (HgCdTe) detector (ViGO UHSM-10.6) photovoltaic detector. The MCT detector converts the incoming optical signals to electrical signals. It is coupled with a Peltier module and has a built-in transimpedance amplifier (TIA). The operational temperature of the MCT detector is 200 K. The electrical signal passes through an external electrical amplifier and is converted to digital samples by a 40 GSa/s real-time digital storage oscilloscope (DSO) for offline DSP routine on the receiver-side (Rx) for demodulation. The Rx DSP begins with a matched RRC filter for up-sampling and then timing recovery. Afterward, the digital samples are subjected to down-sampling based on maximum variance criteria, followed by a symbol-spaced adaptive DFE to mitigate the effects of inter-symbol interference (ISI) and other systematic errors caused through the link. After symbol demodulation, the recovered data sequence is compared with the transmitted data to compute the BER.

Optics EXPRESS

2.2. Characteristics of the laser and the detector

The directly modulated QCL (DM-QCL) chip is a distributed feedback (DFB) laser with the waveguide length of 4 mm that is fabricated by mirSence. The QCL emits at the center wavelength of 9.1 µm and functions in continuous-wave (CW) mode at room temperature and is mounted on Peltier thermoelectric cooling (TEC) to ensure a steady operational temperature, maintaining stability at both 15°C and 20°C settings. The DM-QCL is grown via molecular beam epitaxy (MBE) on an InP cladding, with the active region structured with a strain-compensated AlInAs/GaInAs composition of barriers and wells [31]. Using a buried configuration, the laser went through ridge waveguide etching followed by regrowth of Iron-doped InP to satisfy the criteria for CW operation at room temperature. Finally, the laser is mounted epi-down on a copper block. We characterize the P-I-V curve of the QCL chip, which is measured at operating temperatures of 15°C (288.15 K) and 20°C (293.15 K), as demonstrated in Fig. 2(a), providing information regarding the chip's power output and current consumption at the designated temperatures. At 15°C, the DM-QCL laser indicates a lasing threshold of approximately 420 mA under CW operation and saturates at around 520 mA. The lasing threshold tends to rise slightly with higher operating temperatures at 20°C, which is 440 mA, and the saturation occurs around the same current bias point as 15°C. Operating beyond 520 mA has potential damage from overdriving. When the laser bias current turns up to 520 mA, the QCL has an output power of 9.63 mW at 15°C and 9.08 mW at 20°C. Figure 2(b) shows the normalized spectra of the QCL chip at different bias current points, i.e., 500 mA, 570 mA, and 630 mA, measured at 15°C. The current-tuning coefficient for the DM-QCL is determined around 264 MHz/mA, which explicates the wavelength shift of the laser emission concerning variations in the injection current. Beyond the saturation threshold, the QCL's output power stabilizes or decreases due to factors such as thermal effects and non-linearity. These spectra not only provide a comprehensive understanding of the QCL's behavior under various operating conditions but also highlight how the emission characteristics evolve and the performance limitations when the QCL is driven beyond its optimal operating point. While this QCL shows notable performance, particularly in terms of stability and design innovation. However, when compared to the benchmarks set by state of the art, it becomes clear that there is room for further enhancement. Recent research by Gao et al. highlights a high bandwidth DM-QCL at 8.5 µm, integrated with a grounded coplanar waveguide transmission line, with 16.5 GHz modulation bandwidth in CW mode at room temperature [32].

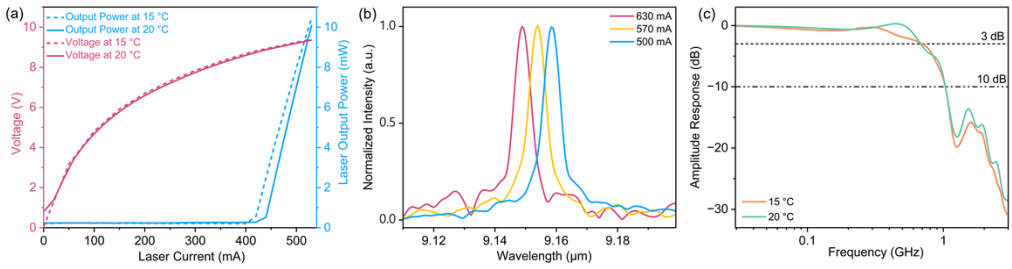

Fig. 2. (a) The measured P-I-V curves of the QCL chip at operating temperatures of 15°C and 20°C. (b) The measured optical spectra with normalized intensity with respect to the bias current of the DM-QCL at 15°C. (c) Characterized end-to-end amplitude response of the entire system (AWG, DM-QCL, MCT, DSO, and all other electronic components).

Figure 2(c) presents the calibrated end-to-end channel amplitude response of the FSO system, with the laser operating at 15°C and 20°C, including the AWG, the DM-QCL, the MCT detector, the DSO, and all the electrical components. A single-tone sweep is conducted to scan frequencies up to 3 GHz. The end-to-end 3-dB bandwidth is measured at 690 MHz, and the 10-dB bandwidth is at 1.02 GHz. The frequency response remains consistent across two laser temperature settings,

Optics EXPRESS

demonstrating similar values. While the TEC module successfully achieves a lower operating temperature of 15°C for the laser, it doesn't significantly enhance the system bandwidth due to limitations in MCT performance. However, the MCT detector provides superior noise performance, thereby improving the overall performance of the FSO transmission. The limited bandwidth of the end-to-end FSO system can lead to significant frequency roll-off in transmitted signals at high data rates. To address this, we employed the pre-emphasis filter at the transmitter. Per the MCT vendor's datasheet, the detectivity spectrum of the MCT detector with respect to wavelength shows that it covers a wide operational spectral range in the 3-12 μm window over MWIR to LWIR at room temperature. The bandwidth of the MCT detector is 1.2 GHz. MCT detectors are commercially available with fine-tuned collimation and low thermal noise performance [33]. They are often integrated with TIA, enhancing conversion efficiency and achieving a higher SNR on the receiver side. They are also compatible with a variety of optical accessories, facilitating easy integration into diverse setups [21].

3. Results and discussion

3.1. BER evaluation with laser bias current variations

We calculated the BER results to inspect the system transmission performance and check the reliability of the FSO link with three modulation formats: NRZ-OOK, PAM4, and PAM6. We performed consecutive sweeps of laser bias currents at two specific temperature settings of the laser, 15°C, and 20°C. By maintaining a constant power into the MCT detector, we ensured that the intensity of the laser beam reaching the MCT remained consistent throughout the experiment. This sweep explores the balance between the modulation depth and modulation linearity. There is a trade-off between achieving higher modulation depth for better signal robustness and maintaining modulation linearity for accurate recovery of the modulated signal. We evaluated the highest bit rates with achievable BER after the DFE-based post-processing, against three benchmarks: the KR-FEC limit of 1.44×10^{-5} [34], the 6.25%-OH HD-FEC threshold of 4.5×10^{-3} BER [35], and the 20%-OH soft-decision FEC (SD-FEC) limit of 2×10^{-2}, which offers more significant coding gain that could effectively reduce errors in data transmission. However, it comes with drawbacks, such as increased complexity and latency. In such scenarios, where communication spans over long distances and is susceptible to atmospheric disturbances, robust error correction mechanisms like SD-FEC can minimize the need for re-transmission, thereby improving overall reliability [36].

Figure 3(a) shows the BER results as a function of laser bias current at the laser operating at 15°C for different modulation formats. For 10 Gbaud NRZ-OOK, we achieved a BER significantly below the KR-FEC threshold. The corresponding eye diagram is shown in the inset, revealing a distinct eye opening for clear observation. This setup yields a net bitrate of 9.7 Gbps. The 16 Gbaud NRZ-OOK and 9 Gbaud PAM4 configurations achieved BER below the 6.25%-OH HD-FEC limit, resulting in net bitrates of 15 Gbps and 16.9 Gbps, respectively. Compared to the 20%-OH SD-FEC, the system can support up to 8 Gbaud PAM6, resulting in a net bitrate of 16.6 Gbps. The corresponding eye diagrams for 8 Gbaud PAM6 and 9 Gbaud PAM4 are displayed in the inset. The eye diagram of PAM6 displayed subtle compression on its upper and lower edge levels. This compression occurred due to the stringent SNR requirement, which forced the driving signal to undergo a substantial peak-to-peak voltage swing. Figure 3(b) exhibits the BER outcomes as a function of laser bias current at the laser operating at 20°C for different modulation formats. We achieved 15 Gbaud NRZ-OOK, 9 Gbaud PAM4, and 7 Gbaud PAM6 configurations. Each one successfully met the 6.25%-OH HD-FEC threshold, yielding net bitrates of 14.1 Gbps, 16.9 Gbps, and 16.4 Gbps, respectively. The corresponding eye diagrams are distinctly separated and appear in the inset. It is evident that PAM4 emerges as the optimal modulation format for both temperature settings. We observed that increasing the laser bias current enhances the BER performance. This improvement is attributed to the

Optics EXPRESS

higher output power, which boosts the SNR and enhances the overall fidelity of the received signal. However, while this parameter adjustment results in better BER outcomes, it is not solely sufficient for achieving optimal transmission performance with advanced modulation formats such as PAM6. Optimal performance also requires careful attention to modulation linearity, the bandwidth of the system, and channel SNR. To further optimize the transmission, it is imperative to employ advanced equalization techniques that can effectively counteract channel impairments and improve signal processing. Additionally, optimizing the design of the photodetector to better match the increased power output and sensitivity requirements can significantly contribute to minimizing errors and enhancing system reliability.

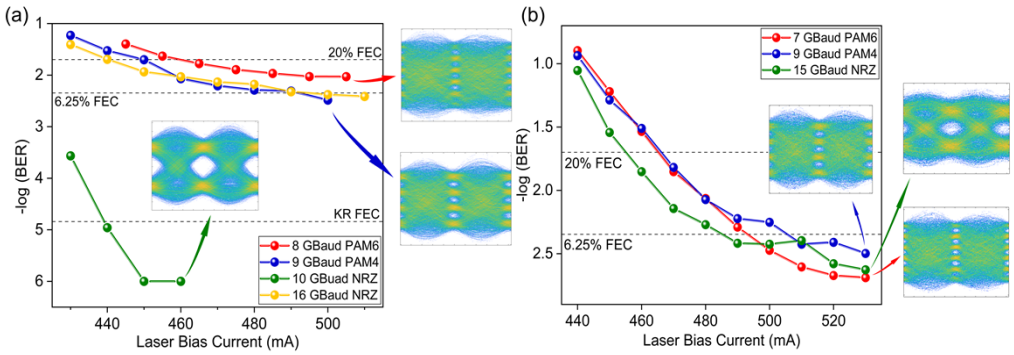

Fig. 3. (a) BER results with respect to laser bias current for different modulation formats at the laser's operating at 15°C. Insets: Selected eye diagram for 8 GBaud PAM6, 9 GBaud PAM4, and 10 GBaud NRZ-OOK. (b) BER results with respect to laser bias current for different modulation formats at the laser's operating at 20°C. Insets: Selected eye diagram for 7 GBaud PAM6, 9 GBaud PAM4, and 15 GBaud NRZ-OOK.

3.2. BER evaluation with DFE tap number variations

We investigate the FSO transmission performance using the three modulation formats: NRZ-OOK, PAM4, and PAM6. Employing DFE-based post-equalization helps mitigate signal distortions induced by bandwidth-limited links. For simplicity and better performance, the number of DFE taps remained constant throughout all test cases. However, exploring other scenarios is possible. Figure 4 details a thorough analysis of the impact of DFE taps on BER performance. Figure 4(a) shows BER performance as a function of DFE tap number at 10 Gbaud NRZ-OOK data rate at the laser operating at 15°C. For 10 Gbaud NRZ-OOK, DFE consisting of only 13 feedforward (FF) taps is effective and operational below the 6.25%-OH HD-FEC threshold. BER performances below the KR-FEC limit are attainable with a DFE comprising 77 FF taps and 3 feedback (FB) taps. Figure 4(b) exhibits BER performance for 16 Gbaud NRZ-OOK as a function of DFE tap number at 15°C. At this symbol rate, achieving the 6.25%-OH HD-FEC limit is crucial for reliable data transmission. This can be accomplished with either a DFE comprising 99 FF taps and 55 FB taps, or with 77 FF taps and 77 FB taps. Both configurations effectively mitigate Intersymbol Interference (ISI) and enhance error correction capabilities, ensuring reliable communication even at high symbol rates. We then extend our system performance evaluation with multilevel PAM signals. PAM4 offers increased spectral efficiency, allowing for higher data throughput within the same bandwidth, and is better suited for long-distance high-speed communication due to its resilience to channel impairments like chromatic dispersion. The corresponding BER performance against the 20%-OH SD-FEC benchmark is achievable via DFE of 33 FF and 13 FB taps. Figure 4(c) shows BER performance for 9 Gbaud PAM4 modulation as a function of DFE tap number at 15°C. The system achieved 6.25%-OH HD-FEC using DFE configuration

Optics EXPRESS

consisting of 77 FF and 77 FB taps. Considering the complexity of PAM4 signals and their heightened susceptibility to noise, this DFE ensures comprehensive compensation for signal distortions caused by channel impairments. The 20%-OH SD-FEC can be reached by employing either a DFE of 33 FF taps and 13 FB taps or a configuration with 99 FF taps and 3 FB taps. Figure 4(d) shows the BER performance of 8 Gbaud PAM6 modulation as a function of DFE tap number at 15°C. It indicates that using DFE of 77 FF and 55 FB taps could achieve data transmission below the 20%-OH SD-FEC threshold. Employing the DFE with larger FB taps effectively reduces Intersymbol Interference (ISI) in PAM6 signals due to the limited bandwidth in LWIR FSO systems.

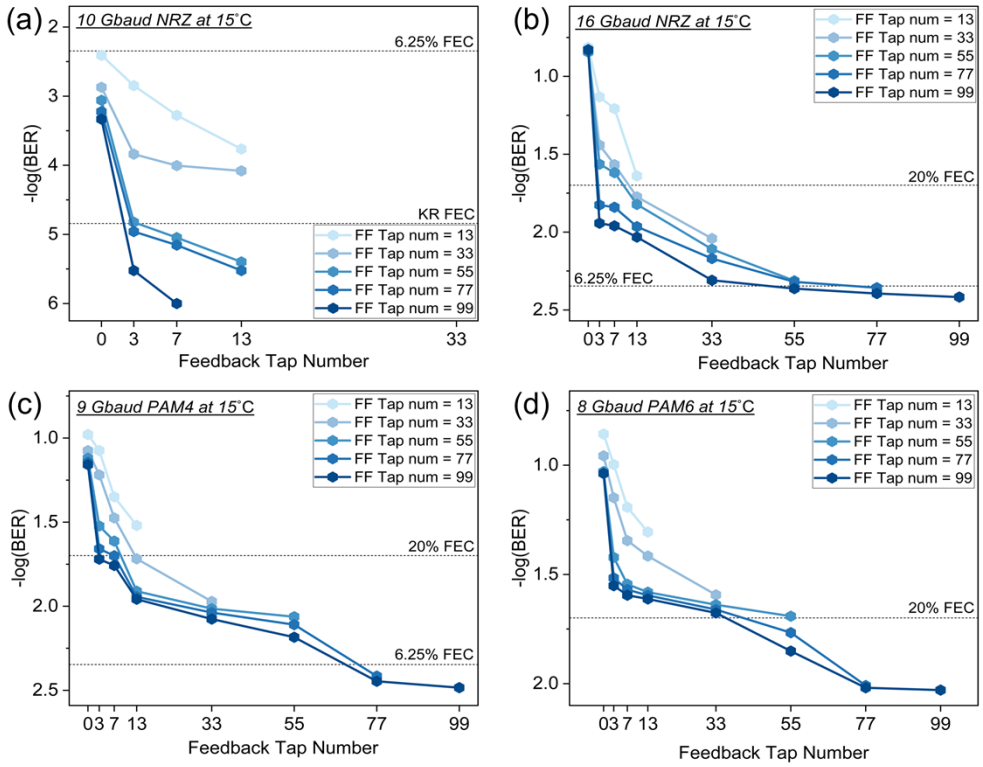

Fig. 4. BER performance as a function of DFE tap number at the laser operating at 15°C. (a) 10 Gbaud NRZ-OOK. The 6.25% overhead HD-FEC limit can be achieved with DFE of 13 feedforward (FF) taps. The KR-FEC limit can be obtained with DFE of 77 FF taps and 3 feedback (FB) taps. (b) 16 Gbaud NRZ-OOK, The HD-FEC limit can be achieved with either DFE of 99 FF taps plus 55 FB taps, or 77 FF taps plus 77 FB taps. (c) 9 Gbaud PAM4. The HD-FEC can be achieved with 77 FF taps plus 77 FB taps. (d) 9 Gbaud PAM4. The 20% overhead SD-FEC limit can be achieved with 77 FF taps plus 55 FB taps.

Figure 5(a) demonstrates in detail the BER performance for 15 Gbaud NRZ-OOK modulation as a function of DFE tap number at the laser operating at 20°C. The 6.25%-OH HD-FEC limit can be attained through two options. One employs DFE composed of 77 FF taps alongside 33 FB taps. Alternatively, achieving the exact limit is possible with a setup consisting of 55 FF taps and 55 FB taps. Regarding the 20%-OH SD-FEC threshold, the best BER result is obtained through either 55 FF and 3 FB taps or with 33 FF and 7 FB taps. It is evident that after 33 feedback taps, the BER counts remain nearly flat. Figure 5(b) shows the BER performance for 9 Gbaud PAM4 modulation relative to the number of DFE taps at 20°C. At this data rate, reaching the 6.25%-OH HD-FEC is feasible by using DFE of 77 FF and 77 FB taps. DFE with 77 FF

Optics EXPRESS

taps and 3 FB taps is enough to ensure BER performance below the 20%-OH SD-FEC limit. Figure 5(c) illustrates the BER evaluation with respect to DFE tap number at 20°C for the data rate of 7 Gbaud PAM6. Meeting the 6.25%-HD HD-FEC threshold is attainable by using a DFE setup consisting of 55 FF taps combined with 55 FB taps. Exceeding 55 feedback taps does not improve the result any further. Utilizing DFE formed by only 77 feedforward taps is effective in maintaining functionality below the 20%-OH SD-FEC limit.

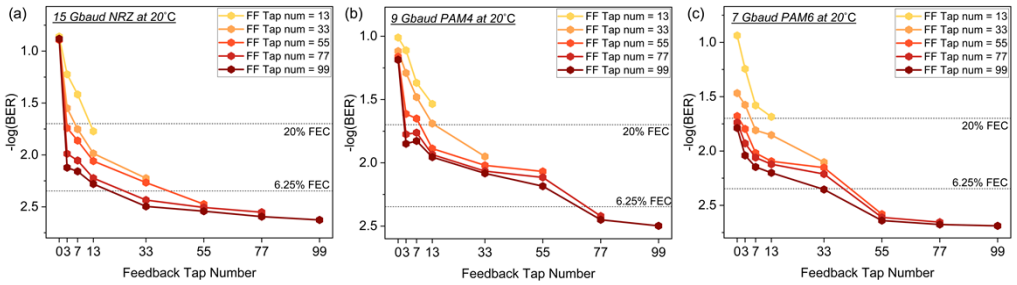

Fig. 5. BER performance as a function of DFE tap number at the laser operating at 20°C. (a) 15 Gbaud NRZ-OOK. The 6.25% overhead HD-FEC limit can be achieved with either DFE of 77 feedforward (FF) taps plus 33 feedback (FB) taps, or 55 FF taps and 55 FB taps. (b) 9 Gbaud PAM4, The HD-FEC limit can be achieved with DFE of 77 FF taps plus 77 FB taps. (c) 7 Gbaud PAM6. The HD-FEC can be achieved with 55 FF taps plus 55 FB taps.

4. Conclusions

We demonstrate a 9.1 µm DM-QCL-based LWIR FSO links and a commercial MCT detector, achieving net bitrates of NRZ-OOK, PAM4, and PAM6. The system supports net bitrates of 15 Gbps NRZ-OOK and 16.9 Gbps PAM4 at 15°C of laser's operating temperature, and 14.1 Gbps, 16.9 Gbps, and 16.4 Gbps with NRZ-OOK, PAM4, and PAM6, respectively, at 20°C achieved BER below the 6.25%-OH HD-FEC limit, all achieving below the 6.25%-OH HD-FEC limit performance. In addition, we achieved a net bitrate of 9.7 Gbps with a BER remarkably below the KR-FEC threshold. This accomplishment exceeds the previous records employing DM-QCL and MCT detector and highlights the potential of LWIR FSO systems as integral components of future information and communication technology (ICT) infrastructure. In our future work, we will focus on enhancing laser safety measures, exploring higher data rates, and extending transmission distances in the LWIR spectrum. Furthermore, we anticipate broader exploration into all-spectra communication paradigms, particularly utilizing LWIR technology alongside advancements in ultrafast mid-IR photodetectors and high-speed modulation techniques. We aim to achieve higher transmission data rates, extending from the LWIR to the terahertz (THz) region, thereby influencing the future landscape of optical communication systems.

Funding. Horizon 2020 Framework Programme cFLOW project (828893); Vetenskapsrådet (2019-05197); Project 'BRAIN' (2022-04798); EU COST Action CA19111 NEWFOCUS; The LZP FLPP Project 'MIR-FAST' (lzp-2023-1-0503); The Strategic innovation program smarter electronic systems - a joint venture by Vinnova, Forms and the Swedish Energy Agency A-FRONTHAUL Project (2023-00659).

Disclosures. The authors declare no conflict of interest.

Data availability. The data that support the findings of this study are available from the corresponding author upon reasonable request.

References

1. X. You, C.-X. Wang, J. Huang, *et al.*, "Towards 6 G wireless communication networks: vision, enabling technologies, and new paradigm shifts," Sci. China Inf. Sci. **64**(1), 110301 (2020).

Optics EXPRESS

2. X. Pang, O. Ozolins, S. Jia, *et al.*, "Bridging the terahertz gap: photonics-assisted free-space communications from the submillimeter-wave to the mid-infrared," J. Lightwave Technol. **40**(10), 3149–3162 (2022).
3. M. A. Khalighi and M. Uysal, "Survey on free space optical communication: a communication theory perspective," IEEE Commun. Surv. Tutorials **16**(4), 2231–2258 (2014).
4. J. J. Liu, B. L. Stann, K. K. Klett, *et al.*, "Mid and long-wave infrared free-space optical communication," presented at the *Laser Communication and Propagation through the Atmosphere and Oceans VIII* (2019).
5. A. Trichili, M. A. Cox, B. S. Ooi, *et al.*, "Roadmap to free space optics," J. Opt. Soc. Am. B **37**(11), A184 (2020).
6. X. Zhu and J. M. Kahn, "Free-space optical communication through atmospheric turbulence channels," IEEE Trans. Commun. **50**(8), 1293–1300 (2002).
7. T. G. Mayerhofer, S. Pahlow, and J. Popp, "Recent technological and scientific developments concerning the use of infrared spectroscopy for point-of-care applications," Spectrochim. Acta, Part A **251**, 119411 (2021).
8. H. Dely, M. Joharifar, X. Pang, *et al.*, "High bitrate data transmission in the 8-14 microm atmospheric window using an external Stark-effect modulator with digital equalization," Opt. Express **31**(5), 7259–7264 (2023).
9. E. Leitgeb, T. Plank, M. S. Awan, *et al.*, "Analysis and evaluation of optimum wavelengths for free-space optical transceivers," presented at the *International Conference on Transparent Optical Networks*, 2010.
10. K. Zou, K. Pang, H. Song, *et al.*, "High-capacity free-space optical communications using wavelength- and mode-division-multiplexing in the mid-infrared region," Nat. Commun. **13**(1), 7662 (2022).
11. O. Spitz, P. Didier, L. Durupt, *et al.*, "Free-space communication with directly modulated mid-infrared quantum cascade devices," IEEE J. Sel. Top. Quantum Electron. **28**(1: Semiconductor Lasers), 1–9 (2022).
12. C. Sauvage, C. Robert, B. Sorrente, *et al.*, "Study of short and mid-wavelength infrared telecom links performance for different climatic conditions," presented at the *Environmental Effects on Light Propagation and Adaptive Systems II*, 2019.
13. B. Hinkov, F. Pilat, L. Lux, *et al.*, "A mid-infrared lab-on-a-chip for dynamic reaction monitoring," Nat. Commun. **13**(1), 4753 (2022).
14. D. Jung, S. Bank, M. L. Lee, *et al.*, "Next-generation mid-infrared sources," J. Opt. **19**(12), 123001 (2017).
15. N. Mustafa, L. Pesquera, C. Cheung, *et al.*, "Terahertz bandwidth prediction for amplitude modulation response of unipolar intersubband semiconductor lasers," IEEE Photonics Technol. Lett. **11**(5), 527–529 (1999).
16. X. Pang, R. Schatz, M. Joharifar, *et al.*, "Direct modulation and free-space transmissions of up to 6 Gbps multilevel signals with a 4.65 μm quantum cascade laser at room temperature," J. Lightwave Technol. **40**(8), 2370–2377 (2022).
17. F. Cheng, J. Zhang, Y. Guan, *et al.*, "Ultralow power consumption of a quantum cascade laser operating in continuous-wave mode at room temperature," Opt. Express **28**(24), 36497–36504 (2020).
18. P. Didier, H. Knötig, O. Spitz, *et al.*, "Interband cascade technology for energy-efficient mid-infrared free-space communication," Photonics Res. **11**(4), 582 (2023).
19. H. Dely, T. Bonazzi, O. Spitz, *et al.*, "10 Gbit s−1 free space data transmission at 9 μm wavelength with unipolar quantum optoelectronics," Laser Photonics Rev. **16**, 1 (2021).
20. E. Rodriguez, A. Mottaghizadeh, D. Gacemi, *et al.*, "Room-temperature, wide-band, quantum well infrared photodetector for microwave optical links at 4.9 μm Wavelength," ACS Photonics **5**(9), 3689–3694 (2018).
21. M. Han, M. Joharifar, M. Wang, *et al.*, "High spectral efficiency long-wave infrared free-space optical transmission with multilevel signals," J. Lightwave Technol. **41**(20), 6514–6520 (2023).
22. L. Gendron, M. Carras, A. Huynh, *et al.*, "Quantum cascade photodetector," Appl. Phys. Lett. **85**(14), 2824–2826 (2004).
23. M. Joharifar, H. Dely, X. Pang, *et al.*, "High-Speed 9.6-μm long-wave infrared free-space transmission with a directly-modulated QCL and a fully-passive QCD," J. Lightwave Technol. **41**(4), 1087–1094 (2023).
24. M. Han, M. Joharifar, M. Wang, *et al.*, "Long-wave infrared discrete multitone free-space transmission using a 9.15-μm quantum cascade laser," IEEE Photonics Technol. Lett. **35**(9), 489–492 (2023).
25. J. A. Lau, V. B. Verma, D. Schwarzer, *et al.*, "Superconducting single-photon detectors in the mid-infrared for physical chemistry and spectroscopy," Chem. Soc. Rev. **52**(3), 921–941 (2023).
26. A. Almogahed, A. Amphawan, and Y. Fazea, "Mitigation of atmospheric turbulences using mode division multiplexing based on decision feedback equalizer for free space optics," J. Opt. Commun. **41**(2), 185–193 (2020).
27. M. Joharifar, M. Han, R. Schatz, *et al.*, "8.1 Gbps PAM8 long-wave IR FSO transmission using a 9.15-μm directly-modulated QCL with an MCT detector," presented at the *Optical Fiber Communications Conference and Exhibition (OFC)*, Th1 H.1, 2023.
28. R. Puerta, M. Han, M. Joharifar, *et al.*, "NR conformance testing of analog radio-over-LWIR FSO fronthaul link for 6 G Distributed MIMO networks," presented at the Optical *Fiber Communication Conference (OFC)*, Th2A.32, 2023.
29. M. Joharifar, H. Dely, L. Durupt, *et al.*, "16.9 Gbps single-channel LWIR FSO data transmission with directly modulated QCL and MCT detector," presented at the Optical *Fiber Communications Conference and Exhibition (OFC)*, Th2A.25, 2024.
30. Y. V. Flores, *Mid-infrared quantum cascade lasers theoretical and experimental studieson temperature-driven scattering*, (Mathematisch-Naturwissenschaftliche Fakultät, 2015).
31. M. Carras, G. Maisons, B. Simozrag, *et al.*, "Room-temperature continuous-wave metal grating distributed feedback quantum cascade lasers," Appl. Phys. Lett. **96**(16), 1 (2010).
32. X. Gao, K. Yang, Y. Zhu, *et al.*, "High frequency mid-infrared quantum cascade laser integrated with grounded coplanar waveguide transmission line," IEEE Electron Device Lett. **45**(4), 649–652 (2024).

Optics EXPRESS

33. J. Piotrowski and A. Piotrowski, "Room temperature IR photodetectors," *Mercury Cadmium Telluride: Growth, Properties and Applications*, (Wiley, 2010), pp. 513–537.
34. "IEEE Standard for Ethernet," in IEEE Std 802.3-2022 (Revision of IEEE Std 802.3-2018).
35. L. M. Zhang and F . R. Kschischang, "Staircase codes with 6% to 33% overhead," J. Lightwave Technol. **32**(10), 1999–2002 (2014).
36. B. Mukherjee, I. Tomkos, M. Tornatore, *et al.*, "Forward error correction for optical transponders," in *Springer Handbook of Optical Networks*, Springer, pp. 177–257, 2020.